Network pharmacology-based strategy to investigate the molecular target and mechanism of Jiawei Linggui Zhugan decoction in the treatment of obesity

Ning Wang
Zhongshan University
Hongda Chen
Zhongshan University
Zhiyu Ye
Zhongshan University
Nan Cao
Zhongshan University
Binyan Mo
Zhongshan University
Jian Qin
Zhongshan University
Li Tan (nitatanli@icloud.com)
Shenzhen Longhua District Central Hospital

Research Article

Keywords: Obesity, Network pharmacology, Jiawei Ling Gui Zhu Gan

Posted Date: October 19th, 2021

DOI: https://doi.org/10.21203/rs.3.rs-982978/v1

Abstract

Background: Jiawei Ling Gui Zhu Gan Decoction (JW-LZD) is based on Linggui Zhugan Decoction (LZD) and adds eight traditional Chinese medicines: *Codonopsis pilosula, Astragalus membranaceus, Yam, Epimedium, Morinda officinalis, Tangerine Peel, Pinellia ternata and Coix Seed*, which can be used for the treatment of obesity in the clinical. However, the pharmacological mechanisms of JW-LZD remain unclear.

Methods: In this study, we determined the molecular targets and mechanisms involved in obesity treatment through network pharmacological analysis, and molecular docking technology. Related compounds were obtained from the TCMSP. Oral bioavailability and drug-likeness were screened using pharmacokinetic criteria. Molecular targets were identified in the drug-bank database and compared with obesity disease differential genes with $P < 0.05$ and | log2FC > 0.5 obtained in the GEO-database to obtain cross genes and construct the TCM compound disease regulation network. After constructing PPI, Go, and KEGG analyses, the key active components and target genes were selected. Molecular docking was carried out using AutoDock, and the best binding target was selected to select the best binding target for molecular docking.

Results: A total of 248 potential compounds and 30 strongly associated JW-LZD targets were identified. Pathway enrichment analysis showed that putative JW-LZD targets mostly participated in adenylate cyclase-activating adrenergic receptor signaling, adrenergic receptor signaling, regulation of signal receptor activity, coagulation, and other metabolic related biological processes. The molecular docking results showed that the key JW-LZD components have good potential to combine with the target genes ADRB2, ADRA2A, ADRA2C, CHEK1, CHEK2, and DGAT2.

Conclusion: JW-LZD could prevent obesity through the molecular mechanisms predicted by network pharmacology, providing a way to develop new combination medicines for obesity.

Background

In recent years, obesity has become an increasingly serious public health problem worldwide, and its annual prevalence has sharply increased [1]. Obesity can also lead to a variety of chronic diseases, such as type 2 diabetes, liver fat, cardiovascular disease, hypertension, stroke, dyslipidaemia, and many other diseases [2]. In 2016, the World Health Organization estimated that 1.9 billion adults were overweight, of which 650 million were obese[3–5]. Therefore, obesity treatment is imminent, but effective treatment is still lacking.

TCM is a comprehensive medicinal system that plays a key role in health maintenance for Asian people, and has gradually gained popularity in Western countries because of its reliable therapeutic efficacy and fewer side effects. Based on the theory of traditional Chinese herbal medicine, TCM offers bright prospects for the systematic prevention and treatment of complex diseases.

Linggui Zhugan Decoction (LZD) comes from “Treatise on Febrile Diseases”, and the Jiawei Linggui Zhugan decoction (JW-LZD) is based on LZD decoction, which adds other drugs for warming yang, supplementing qi, strengthening spleen, and removing dampness. It is composed of 12 traditional Chinese medicines, including *Poria cocos*, cinnamon twig, *Atractylodes macrocephala*, lcorice, *Codonopsis pilosula, Astragalus*, yam, *Epimedium, Morinda officinalis*, tangerine peel, *Pinellia ternata*, and coix. Several clinical studies showed that JW-LZD combined with short-term fasting significantly reduced body weight, waist circumference, and triglyceride levels in obese patients. It also has a synergistic therapeutic effect on fatty liver and diabetes with obesity, and has good safety and feasibility[6–10]. Although well-practiced in clinical medicine, very little is known about the active substances and specific molecular mechanisms of JW-LZD acting on obesity.

Similar to other TCM formulas, JW-LZD is a multi-component and multi-target agent that achieves its specific therapeutic efficacy through active components that regulate molecular networks within the body. Therefore, it is difficult to investigate the pharmacological mechanisms of JW-LZD in obesity treatment.

Network pharmacology is a combination of pharmacology, bioinformatics, and other sciences with system network analysis. By constructing a network related to "disease phenotype gene drug", it explains the multi-component and multi-target drug treatment mechanism from the aspects of gene distribution, molecular function and signal pathway. It is suitable for research on traditional Chinese medicinal compounds.

In this study, we aimed to use a comprehensive network pharmacology-based approach to investigate the mechanisms underlying the therapeutic effects of JW-LZD on obesity.

Methods

Chemical ingredients database building

We performed a search using the 2014 updated Traditional Chinese Medicine Systems Pharmacology Database (TCMSP, http://lsp.nwu.edu.cn/tcmsp.php, updated on May 31, 2014) to screen the chemical ingredients of the 12 herbs contained in JW-LZD, with drug-like properties (DL) ≥ 0.18, and oral bioavailability (OB) ≥ 30%. The predicted targets of the screened compounds were acquired from the DrugBank(https://www.drugbank.ca/) database. Meanwhile, the UniProt database(https://www.uniprot.org/) was used to compare the target information and gene name standardisation.

The acquisition of obesity differential genes

We acquired differentially expressed gene samples (GSE9642) from healthy and obese patients in the GEO database (https://www.ncbi.nlm.nih.gov/geo/). The script runs in Perl (Strawberry Perl-5.30.2.1) software, and the gene probe names were

annotated as gene symbols and grouped. The “limma” package was installed in the Perl software, and the sample values were corrected and subjected to log2 (logFC) transformation. Samples with $P < 0.005$ and $|\log2\ FC| > 1$ were considered statistically significant. The gene volcano map of the samples was generated, and the top 20 genes with the most significant up- and down-regulation were selected in creating the heat map.

TCM Compound-Disease Regulatory Network.

The Perl software was used to acquire the target genes of TCM and the active ingredients of TCM, as well as the intersection genes of the disease differential genes. Then, the TCM compound-disease regulatory network was generated using Cytoscape (version 3.7.2).

Protein–Protein Interaction Network (PPI) and Topological Analysis.

The “Bisogenet, CytoNAC” package was installed in Cytoscape, and the intersection genes were entered, and the parameter “homo sapiens” was selected. Data for constructing the PPI network were sourced from six main experimental research databases: human protein reference, molecular interaction, interacting proteins, biological general repository for interaction, biomolecular interaction network, and intact molecular interaction. The method “input nodes and its neighbors” was selected to obtain the PPI network and perform topological analysis based on its network centrality.

KEGG and Go enrichment Analysis.

The “stringi”, “colorspace”, and “ggplot2” packages were installed in R (version 3.6.3). Bioconductor packages, including “cluster Profiler”, “DOSE”, and “enrichplot” were used for GO and KEGG enrichment analyses. The “enrichGO” function was used for GO enrichment analysis and the “enrich-KEGG” function was used for KEGG enrichment analysis. As for the parameters of the two functions, species was set to “has” and the filter values were set to $P < 0.05$ and $q < 0.05$. The first 20 enrichment results were visualised as a bar graph, and the KEGG regulatory network was generated using Cytoscape.

Molecular Docking.

The target genes involved in the first nine pathways of the KEGG enrichment results were searched in the PDB database (https://www.rcsb.org), of which the 3D protein conformations with a crystal resolution of less than 3 Å as determined by X-ray crystal diffraction were acquired. 3DSDF format files of JW-LZD key active ingredients were downloaded from the PubChem platform.

PyMOL and Auto-Docktools (version 1.5.6) were used to remove protein water molecules and ligands and select corresponding proteins and ligands, respectively. The docking box was adjusted to include all the protein structures, and the ligand coordinates were recorded. According to the algorithm created by Trott et al. [9], AutoDock Vina (version 1.1.2) was used to run, and finally, the molecular docking binding energy was obtained. PyMOL was used to generate the local diagram of molecular docking.

Results

Active Ingredients of JW-LZD

In the TCMSP database, the active components of JW-LZD were screened with OB ≥ 30% and DL ≥ 0.18. JW-LZD contains 248 active ingredients, including 15, 7, 7, 92, 21, 20, 16, 23, 20, 5, 13, and 9 in *P. cocos, cinnamon twig, A. macrocephala, licorice, dangshen, Astragalus, yam, Epimedium, M. officinalis, tangerine peel, P. ternata, and coix seeds,* respectively (Table 1).

Differential Gene Screening

By comparing eight normal samples and seven disease samples from the GEO database, 21654 differential genes were obtained, including 10872 up-regulated genes and 10782 down-regulated genes, of which 597 and 434 were statistically significant, respectively. As shown in the gene volcano map (Figure. 1), the differentially expressed genes in the disease samples were normally distributed, with a larger number of significantly up-regulated genes than significantly down-regulated genes. Figure. 2 and Table 2 list the top 20 genes with the most significant up-and down-regulation.

Construction of the TCM Compound-Disease Regulatory Network.

As listed in Table 3, there are 13 cross genes (sorted by logFC). The targeting relationship between active components of TCM and intersection genes is presented by TCM compound-disease regulation network (Figure. 3). Active ingredients of Licorice and Epimedium have the most effective components and the most related target genes, indicating that Licorice and Epimedium in JW-LZD are the most effective components. The active ingredients quercetin, stigmasterol, 7-o-methylisoxylitol and anhydroicaritin were associated with 7, 3, 3 and 2 target genes, therefore, they are divided into multi-target and multi effect compounds. The gen Chek1 is the gene related to the highest number of active compounds as listed in Table 3, there were 13 cross genes (sorted by logFC). The targeting relationship between the active components of TCM and intersection genes is presented by the TCM compound-disease regulation network (Figure. 3). The active ingredients of licorice and Epimedium were the most effective

components and the most related target genes, indicating that they were the most effective components. The active ingredients quercetin, stigmasterol, 7-o-methylisoxylitol, and anhydroicaritin were associated with seven, three, three, and two target genes, respectively, and were therefore divided into multi-target and multi-effect compounds. The CHEK1 gene was related to the highest number of active components, followed by the adrenoreceptors ADRB2, ADRA2C, and ADRA2A.

PPI Network and Topological Analysis.

In the PPI network, the degree centrality (DC) of a node is the number

of edges it has, with higher degrees indicating more centrality. Betweenness centrality (BC) captures the extent to which a given node is. Specifically, it is the ratio of the number of shortest paths passing through the node to the total number of shortest paths in the network. DC and BC reflect the influence of the corresponding node in the entire network. They described topological centrality based on the connectivity and controllability of the network. The combination of DC and BC values has been confirmed to be effective for screening reliable and important

proteins. As shown in Figure. 4, 580 protein nodes and 6110 edges were obtained for the intersection genes. After screening with DC > 61 and a BC range of 0–113.2, the first 30 proteins are shown in Table 4 (in descending order of degrees), with a total of 248 edges. Among them, nine were predicted targets of the active ingredients, including ADRB2, TP53, FN1, UBC, YWHAZ, FBXO6, COPS5, CHEK2, HSP90AA1, ITGA4, ADRB2, and CHEK1.

GO and KEEG Enrichment Analysis

GO enrichment analysis revealed three levels of gene function: biological process (BP), cellular component (CC), and molecular function (MF). BP mainly involves the activation of adrenergic receptor signalling pathway by adenylate cyclase, adrenergic receptor signalling pathway, coagulation, and haemostasis; MF is mainly involved in adrenergic receptor activity, catecholamine binding, G protein-coupled amine receptor activity, oxidoreductase activity, and so on. The CC showed no involvement (Figure. 5). According to the results of KEGG enrichment, the mechanism of JW-LZD in obesity treatment mainly focuses on the cyclic guanosine acid PKG pathway, P53 pathway, complement and coagulation cascades, neuroactive ligand-receptor interaction, neuroactive ligand-receptor interaction, and cell cycle (Figure. 6). The genes associated with the greatest number of pathways were ADRB2, ADRA2C, ADRA2A, CHEK1, and CHEK2 (Figure. 7 and Table 5).

Molecular Docking Analysis

Molecular docking techniques mimic the interaction between small ligand molecules and receptor protein macromolecules, and the binding energy between the two counterparts can be calculated to predict their affinity. A binding energy < 0 indicates that the two molecules combine spontaneously, and that smaller binding energies lead to more stable conformations. Most of the components in JW-LZD can combine well with the target genes, among which the binding properties of phaseolin, dehydrated icariin, quercetin,

and stigmasterol were the best (Table 6). The genes ADRB2, DGAT2, ADRA2A, ADRA2C, CHEK2, NQO1, and CHEK1 can dock well with the most active ingredients. Figure. 8 illustrates some local structures of molecular docking in detail.

Discussion

In the present network pharmacological analysis, the drug components of 12 TCMs in

JW-LZD and obesity disease target were analyzed by network pharmacology.

stigmasterol, 7-o-methylisoxylitol and anhydroicaritin were identified as active

components related to most targets, and molecular docking analysis also confirmed

that they have good binding characteristics with most target genes.

Quercetin is a naturally abundant polyphenol and flavonoid. It widely

exists in fruits, vegetables, and herbs, which are considered to be the most effective scavengers of reactive oxygen species and can inhibit the production of a variety of proinflammatory factors such as TNF-α and NO[11] and and regulate ochratoxin A-induced oxidative stress and redox signals[12]. I In obesity treatment, quercetin reduces intracellular oxidative stress, reduces chronic low-grade inflammation, inhibits adipogenesis, and inhibits the differentiation of preadipocytes into mature adipocytes[13]. In cell research, quercetin can induce lipolysis of primary rat adipocytes in adose -and time-dependent manner by increasing cyclic adenosine monophosphate levels and hormone-sensitive lipase activity[14]. Additionally, quercetin can significantly reduce the levels of ANGPTL4, adiponectin, PAI-1, and glycolysis-related enzymes ENO2, PKFP, and PFKFB4 in human SGBS adipocytes[15]. Animal studies have shown that quercetin can protect mice or rats from weight gain and adipose tissue accumulation caused by high-fat diet (HFD)[16, 17], and has a beneficial effect on improving HFD-induced obesity and reducing intestinal microbiota imbalance[18]. Recent clinical trials of quercetin on obesity have gradually increased, including reports on quercetin-rich onion being beneficial for preventing obesity and improving liver function[19]. Quercetin supplementation also reduces resistin plasma levels, gene expression, and testosterone and luteinizing hormone concentrations in overweight or obese patients with polycystic ovary syndrome[20]. In terms of dose, clinical trials found that 100 mg/day of quercetin can significantly reduce the overall fat, especially that in the arm, and reduce the body mass index of overweight or obese subjects[21], while 150-mg doses can reduce waist circumference and triglyceride concentrationn[22]. A high-dose study found that quercetin had no effect on oxidative stress and antioxidant capacity during the 12-week consumption period of high-dose quercetin (500–1000 mg/day) in obese subjects[23].

Phytosterols are known to be plant analogues of cholesterol, which compete with cholesterol for intestinal absorption or regulating proteins, reducing cholesterol levels[24]. At present, more than 200 different phytosterols have been identified, including stigmasterol and phytosterol β- Sitosterol being the

most common[25]. In an animal model of high-fat diet, stigmasterol can reduce the level of plasma cholesterol, inhibit the absorption of intestinal cholesterol and phytosterol, inhibit the synthesis of liver cholesterol and typical bile acids, and increase the expression of liver HMGCoAR mRNA, which is the rate-limiting enzyme of cholesterol biosynthesis, thus reducing the level of liver cholesterol[26–28]. Sterol regulatory element binding proteins (SREBPs) play an important role in regulating lipid homeostasis[29] which control the expression of genes involved in the biosynthesis and uptake of fatty acids, triglycerides, cholesterol, and phospholipids[30]. Stigmasterol inhibits SREBP-2 processing and reduces cholesterol synthesis[31].

Icariin, an effective component of *Epimedium*, is an isoprene flavonoid naturally present in several *Epimedium* plants (*Berberidaceae*). Icariin has recently been identified as a new SREBP inhibitor. It can improve diet-induced obesity and reduce insulin resistance by inhibiting the maturation of SREBPs dependent on the LKB1/AMPK/mTOR pathway. It is considered a compound-regulating metabolic disease[32]. 7-o-methylisoxylitol is an effective component extracted from Astragalus[33]. Therefore, the effective drug components in JW-LZD have a definite therapeutic effect on obesity.

The topological analysis results of the PPI network showed that 10 target genes, including ADRB2, TP53, FN1, UBC, YWHAZ, FBXO6, COPS5, CHEK2, HSP90AA1, and ITGA4 are at the core of the network. These 10 target genes not only correspond to multiple active components, but also play an important role in the PPI network, suggesting that they may be a key target for the therapeutic effect of JW-LZD. For example, ADRB2 is a cross gene β2-AR, which is a member of the G protein-coupled receptor superfamily. Polymorphisms, point mutations, and/or downregulation of the gene are associated with nocturnal asthma, obesity, type 2 diabetes, and cardiovascular disease.

The molecular docking analysis results showed that the core targets (ADRB2, ADRA2A, ADRA2C, CHEK1, CHEK2, and DGAT2) and the main active components of JW-LZD (quercetin, stigmasterol, 7-o-methylisoxylitol, and anhydroicaritin) had good docking activity (binding energy < –6.0 kcal/mol), further demonstrating that these components can play a therapeutic role in obesity by regulating the above core targets, confirming the reliability of the above network pharmacological prediction results.

GO enrichment results showed that biological processes are mostly related to adenylate cyclase activating adrenergic receptor signalling pathway and adrenergic receptor signalling pathway, positive regulation of signalling receptor activity, and blood coagulation. In terms of molecular function, the gene is related to metabolism and oxidation reactions such as adrenergic receptor activity, catecholamine binding, G protein-coupled amine receptor activity, and oxidant activity, acting on NADPH, quinone, or similar compounds as acceptors. KEGG enrichment analysis showed that genes were related to the cGMP-PKG signalling pathway, neuroactive live-receiver interaction, and P53 signalling pathway.

From the above biological processes, gene and molecular functions, and KEGG analysis, JW-LZD treatment may be related to regulating the sympathetic nervous system and reducing the inflammatory response.

The adrenergic receptor is a G protein-coupled receptor for catecholamines on the cell surface. They are the basic components of the sympathetic nervous system and jointly participate in the regulation of energy balance and lipid metabolism by the autonomic nervous system (ANS). The decrease in sympathetic excitability may cause weight gain due to a decrease in basal metabolic rate (BMR) and energy consumption[34]. The accumulated white adipose tissue is transformed into brown adipose tissue with energy dissipation. The main endogenous factors are norepinephrine and central sympathetic activators[35]. The adrenergic system plays an important role in regulating energy balance through heat production and lipid mobilisation, and it has been confirmed that adrenergic receptors (β1-AR, β2-AR, and β3-Ar) are involved in the regulation of obesity[36]. It is well-known that the synergistic effect between 3-Ar and uncoupling protein 1(UCP1) is related to weight gain and anti-weight loss, and is highly expressed in white and brown adipocytes and controls the key regulatory pathway of lipid metabolism[36–38]. However, adrenergic stimulation and lipolysis of UCP1 in human brown fat may be mainly mediated by ADRB1[39]. β2-Ar can mediate the production of liver triglycerides and new fat[40], and the β2-ADR gene Arg16Gly and Gln27Glu polymorphisms are associated with plasma total cholesterol and low-density lipoprotein (LDL) cholesterol concentrations[41]. Valet et al.[42] demonstrated that an increased alpha-2/beta-AR balance in adipocytes promotes obesity by stimulating adipocyte hyperplasia.

cGMP is the second messenger involved in the regulation of the cardiovascular system and adipose tissue function[43], which can activate cyclic nucleotide-gated ion channels and cGMP-dependent protein kinase (PKG), which has been identified as the main mediator of the cGMP effect in adipocytes[44]. The cGMP signal can enhance the differentiation of mouse and human adipocytes and activate thermogenic programs. Metabolic inflammation can cause the accumulation of white adipose tissue in the viscera, while the activation of cGMP signalling mediated by sGC-PKG1 can cause a reduction in white adipose tissue in the viscera, and there is no difference in the changes of white adipose tissue in subcutaneous tissue or groin[45].

However, pharmacological studies on the mechanisms and targets of JW-LZD in obesity treatment are limited. Based on our findings, more clinical and animal experiments in the future should be undertaken to assess the relationship between agents used in TCM, including JW-LZD in obesity, and their effects in terms of specific targets at the molecular level to validate the results based on data analysis.

Conclusion

This study aimed to undertake a network pharmacology analysis of the mechanism of the effects of JW-LZD in obesity. The findings showed that quercetin, stigmasterol, 7-o-methylisoxylitol, anhydroicaritin, and other active components in JW-LZD exert its pharmacological effects in obesity by modulating multiple pathways, including adenylate cyclase-activated adrenergic receptor signalling, regulation of signal receptor activity, and coagulation.

However, as this study was based on data mining and data analysis, subsequent experimental analyses should be undertaken on the role of JW-LZD in obesity.

Abbreviations

TCM
Traditional Chinese Medicine
LZD
Linggui Zhugan Decoction
JW-LZD
Jiawei Ling Gui Zhu Gan Decoction
DC
degree centrality
BC
betweenness centrality
BP
biological process
CC
cellular component
MF
molecular function
SREBPs
Sterol regulatory element binding proteins
PPI
Protein–protein interaction
TCMSP
Traditional Chinese Medicine Systems Pharmacology
UCP1
uncoupling protein 1
LDL
low-density lipoprotein
β1-AR
β1adrenergic receptors
β2-AR
β2-adrenergic receptors, and β3-Ar:β3-adrenergic receptors
TNF-α
Tumor necrosis factor alpha

Declarations

Ethics approval

Not applicable.

Consent for publication

Availability of data and materials

The data that support the findings of this study are available from the corresponding author upon request.

Competing interests

The authors declare that they have no competing interests.

Funding

This study was supported by Construction project of characteristic specialty of traditional Chinese medicine in Shenzhen.

Authors' contributions

Li Tan was responsible for the conception and design. Ning Wang were responsible for the development of the methodology. Ning Wang and Hongda Chen, Zhiyu Ye, Nan Cao, Binyan Mo were responsible for the analysis and interpretation of data. Jian Qin and Li Tan were responsible for the writing, review, and revision of the manuscript. Ning Wang and Hongda Chen contributed equally to this work.

Acknowledgements

Ning Wang and Hongda Chen are the co-first author.

References

1. Huh JY, Park YJ, Ham M, Kim JB. Crosstalk between Adipocytes and Immune Cells in Adipose Tissue Inflammation and Metabolic Dysregulation in Obesity. Molecules & Cells. 2014;37(5):365-71.

2. Mayoral L, Andrade GM, Mayoral E, Huerta TH, Perez-Ca Mp Os E. Obesity subtypes, related biomarkers & heterogeneity. The Indian Journal of Medical Research. 2020;151(1):11.

3. Organization WH. Obesity and Overweight. Springer New York. 2011.

4. Jaacks LM, Vandevijvere S, Pan A, McGowan CJ, Wallace C, Imamura F et al. The obesity transition: stages of the global epidemic. Lancet Diabetes Endocrinol. 2019;7(3):231-40. doi:10.1016/s2213-8587(19)30026-9.

5. besity and overweight. https://www.who.int/en/news-room/fact-sheets/detail/

obesity-and-overweight. 2021. Accessed April 2nd 2021.

6. Protective effects of Modified Linggui Zhugan Decoction combined with short-term very low calorie diets on cardiovascular risk factors in obese patients with impaired glucose tolerance. Journal of Traditional Chinese Medicine. 2012;02(v.32):68-73.

7. Bin KE, Shi L, Zhang JJ, Meng J, Chen DS. Clinical research of modified ling-gui-zhu-gan decoction combined with short-term very-low-calorie-diet in treatment of hyperlipidemia combined with fatty liver(splenic hypofunction and dampness accumulation type). Journal of Practical Medicine. 2012;188(5):277-.

8. Chen D, Li C, Michalsen A, Kessler C, Huang Y, Meng J et al. Modified Ling-Gui-Zhu-Gan decoction combined with short-term fasting improves therapeutic response in type 2 diabetic patients. European Journal of Integrative Medicine. 2012;4(3).

9. KE B, L S, JJ Z, J M, DS C. Safety of modified Linggui Zhugan decoction combined with short-term fasting in the treatment of simple obesity. Chinese Journal of Traditional Medical Science and Technology. 2013;20(002):112-4.

10. Yang Y, Li Q, Chen S, Ke B, Huang Y, Qin J. Effects of modified Lingguizhugan decoction combined with weekend fasting on metabolic syndrome. Journal of Traditional Chinese Medicine. 2014;34(1).

11. Sotnikova R, Nosalova V, Navarova J. Efficacy of quercetin derivatives in prevention of ulcerative colitis in rats. Interdisciplinary Toxicology. 2013;6(1).

12. Ramyaa P, Krishnaswamy R, Padma VV. Quercetin modulates OTA-induced oxidative stress and redox signalling in HepG2 cells — up regulation of Nrf2 expression and down regulation of NF-κB and COX-2. Biochimica Et Biophysica Acta. 2014;1840(1):681-92.

13. Zhao Y, Chen B, Jing S, Wan L, Zhu Y, Tao Y et al. The Beneficial Effects of Quercetin, Curcumin, and Resveratrol in Obesity. Oxidative Medicine and Cellular Longevity,2017,(2017-8-24). 2017;2017:1-8.

14. Kuppusamy UR, Das NP. Effects of flavonoids on cyclic AMP phosphodiesterase and lipid mobilization in rat adipocytes. Biochemical Pharmacology. 1992;44(7):1307-15.

15. Andreas L, Kathrin S, Axel M, Christoph S, Elena K, Eva B et al. Quercetin Impacts Expression of Metabolism- and Obesity-Associated Genes in SGBS Adipocytes. Nutrients. 2016;8(5):282.

16. Liang C, Oest ME, Prater MR. Intrauterine exposure to high saturated fat diet elevates risk of adult-onset chronic diseases in C57BL/6 mice. Birth Defects Research Part B Developmental & Reproductive Toxicology. 2010;86(5):377-84.

17. Stewart LK, Soileau JL, Ribnicky D, Wang ZQ, Raskin I, Poulev A et al. Quercetin transiently increases energy expenditure but persistently decreases circulating markers of inflammation in C57BL/6J mice fed a high-fat diet. Metabolism-clinical & Experimental. 2008;57(supp-S1).

18. Le Z, Qi Z, Ma W, Feng T, Shen H, Zhou M. A combination of quercetin and resveratrol reduces obesity in high-fat diet-fed rats by modulation of gut microbiota. Food & Function. 2017;8.

19. Nishimura M, Muro T, Kobori M, Nishihira J. Effect of Daily Ingestion of Quercetin-Rich Onion Powder for 12 Weeks on Visceral Fat: A Randomised, Double-Blind, Placebo-Controlled, Parallel-Group Study. Nutrients. 2019;12(1):91.

20. Khorshidi, Masoud, Moini, Ashraf, Alipoor, Elham et al. The effects of quercetin supplementation on metabolic and hormonal parameters as well as plasma concentration and gene expression of resistin in overweight or obese women with polycystic ovary syndrome. Phytotherapy Research Ptr. 2018.

21. Ji-Sook L, Yong-Jun C, Kyung-Hea L, Jung-Eun Y. Onion peel extract reduces the percentage of body fat in overweight and obese subjects: a 12-week, randomized, double-blind, placebo-controlled study. Nutrition Research & Practice. 2016;10(2):175-81.

22. Pfeuffer M, Auinger A, Bley U, Kraus-Stojanowic I, Laue C, Winkler P et al. Effect of quercetin on traits of the metabolic syndrome, endothelial function and inflammation in men with different \\{APOE\\} isoforms. Nutrition, Metabolism and Cardiovascular Diseases. 2013.

23. Shanely RA, Knab AM, Nieman DC, Jin F, McAnulty SR, Landram MJ. Quercetin supplementation does not alter antioxidant status in humans. Free Radical Research. 2010;44(2).

24. Calpe-Berdiel, Escola-Gil, JC, Blanco-Vaca. New insights into the molecular actions of plant sterols and stanols in cholesterol metabolism. ATHEROSCLEROSIS. 2009;2009,203(1)(-):18-31.

25. Piironen V. Plant sterols: biosynthesis, biological function and their importance to human nutrition. Journal of the Science of Food & Agriculture. 2000;80.

26. Geelen MH, Gibson D, Rodwell V. Hydroxymethylglutaryl-CoA reductase--the rate-limiting enzyme of cholesterol biosynthesis. A report of a meeting held at Nijenrode Castle, Breukelen, The Netherlands, August 24, 1985. Febs Letters. 1986;201(2):183-6.

27. Feng S, Dai Z, Liu AB, Huang J, Nihal N, Guo G et al. Intake of stigmasterol and β-sitosterol alters lipid metabolism and alleviates NAFLD in mice fed a high-fat western-style diet. Biochimica et Biophysica Acta (BBA) - Molecular and Cell Biology of Lipids. 2018;1863:S1388198118302038-.

28. Batta AK, Xu G, Honda A, Miyazaki T, Salen G. Stigmasterol reduces plasma cholesterol levels and inhibits hepatic synthesis and intestinal absorption in the rat. Metabolism-clinical & Experimental. 2006;55(3):292-9.

29. Desvergne, B. Transcriptional Regulation of Metabolism. Physiological Reviews. 2006;86(2):465-514.

30. Wang Y, Viscarra J, Kim SJ, Sul HS. Transcriptional regulation of hepatic lipogenesis. Nature Reviews Molecular Cell Biology. 2015;16(11):678.

31. Yang C, Yu L, Li W, Xu F, Cohen JC, Hobbs HH. Disruption of cholesterol homeostasis by plant sterols. Journal of Clinical Investigation. 2004;114(6):813.

32. Zheng ZG, Zhou YP, Zhang X, Thu PM, Xie ZS, Lu C et al. Anhydroicaritin improves diet-induced obesity and hyperlipidemia and alleviates insulin resistance by suppressing SREBPs activation. Biochemical Pharmacology. 2016:42-61.

33. Subarnas A, Oshima Y, Hikino H. Isoflavans and a pterocarpan from Astragalus mongholicus. Phytochemistry. 1991;30(8):2777-80.

34. Seals DR, Bell C. Chronic sympathetic activation: consequence and cause of age-associated obesity? Diabetes. 2004;53(2):P.276-84.

35. Montanari, T., Poscic, N., Colitti, M. Factors involved in white-to-brown adipose tissue conversion and in thermogenesis: a review. Obesity Reviews An Official Journal of the International Association for the Study of Obesity. 2017.

36. Yasuda K, Matsunaga T, Adachi T, Aoki N, Tsujimoto G, Tsuda K. Adrenergic receptor polymorphisms and autonomic nervous system function in human obesity. Trends in Endocrinology & Metabolism. 2006;17(7).

37. Sivenius K, Valve R, Lindi V, Niskanen L, Laakso M, Uusitupa M. Synergistic effect of polymorphisms in uncoupling protein 1 and beta3-adrenergic receptor genes on long-term body weight change in Finnish type 2 diabetic and non-diabetic control subjects. Int J Obes Relat Metab Disord. 2000;24(4):514-9.

38. Haji E, Mahri SA, Aloraij Y, Malik SS, Mohammad S. Functional Characterization of the obesity-linked variant of the β3-adrenergic receptor. 2021.

39. Ji R, Bjrn R, Meldgaard BJ, Wei L, Hansen JB, Bnlkke PS. Beta-1 and not beta-3-adrenergic receptors may be the primary regulator of human brown adipocyte metabolism. Journal of Clinical Endocrinology & Metabolism. 2019(4):4.

40. Shi Y, Pizzini J, Wang H, Das F, Kamat A. β 2 -Adrenergic Receptor Agonist Induced Hepatic Steatosis in Mice: Modeling Nonalcoholic Fatty Liver Disease in Hyperadrenergic States. AJP Endocrinology and Metabolism. 2021(1).

41. Ukkola O, Rankinen T, Weisnagel SJ, Sun G, Pérusse L, Chagnon YC et al. Interactions among the α2-, β2-, and β3-adrenergic receptor genes and obesity-related phenotypes in the Quebec Family Study. Metabolism-clinical & Experimental. 2000;49(8):1063-70.

42. Valet P, ., Grujic D, ., Wade J, ., Ito M, ., Zingaretti MC, Soloveva V, . et al. Expression of human alpha 2-adrenergic receptors in adipose tissue of beta 3-adrenergic receptor-deficient mice promotes diet-induced obesity. Journal of Biological Chemistry. 2000;275(44):34797-802.

43. Handa P, Tateya S, Rizzo NO, Cheng AM, Morgan-Stevenson V, Han CY et al. Reduced Vascular Nitric Oxide-cGMP Signaling Contributes to Adipose Tissue Inflammation During High-Fat Feeding. Arteriosclerosis, Thrombosis, and Vascular Biology. 2011.

44. Increased cGMP promotes healthy expansion and browning of white adipose tissue. The FASEB Journal. 2013;27(4).

45. Sanyal A, Naumann J, Hoffmann LS, Chabowska-Kita A, Ehrlund A, Schlitzer A et al. Interplay between Obesity-Induced Inflammation and cGMP Signaling in White Adipose Tissue. Cell Reports. 2017;18(1):225.

Tables

Table 1 The total available compounds of MLGZG

Drug	ID	Compound	OB	DL
Atractylodes macrocephala	MOL000072	8β-ethoxy atractylenolide	35.95	0.21
Atractylodes macrocephala	MOL000033	(3S,8S,9S,10R,13R,14S,17R)-10,13-dimethyl-17-[(2R,5S)-5-propan-2-yloctan-2-yl]-2,3,4,7,8,9,11, 12,14,15,16,17-dodecahydro-1H-cyclopenta[a]phenanthren-3-ol	36.23	0.78
Atractylodes macrocephala	MOL000028	α-Amyrin	39.51	0.76
Atractylodes macrocephala	MOL000049	3β-acetoxyatractylone	54.07	0.22
Atractylodes macrocephala	MOL000021	14-acetyl-12-senecioyl-2E,8E,10E-atractylentriol	60.31	0.31
Atractylodes macrocephala	MOL000020	12-senecioyl-2E,8E,10E-atractylentriol	62.40	0.22
Atractylodes macrocephala	MOL000022	14-acetyl-12-senecioyl-2E,8Z,10E-atractylentriol	63.37	0.30
Pericarpium citri reticulatae	MOL000359	sitosterol	36.91	0.75
Pericarpium citri reticulatae	MOL004328	naringenin	59.29	0.21
Pericarpium citri reticulatae	MOL005100	5,7-dihydroxy-2-(3-hydroxy-4-methoxyphenyl)chroman-4-one	47.74	0.27
Pericarpium citri reticulatae	MOL005815	Citromitin	86.90	0.51
Pericarpium citri reticulatae	MOL005828	nobiletin	61.67	0.52
Coix seed	MOL000359	sitosterol	36.91	0.75
Coix seed	MOL000449	Stigmasterol	43.83	0.76
Coix seed	MOL000953	CLR	37.87	0.68
Coix seed	MOL001323	Sitosterol alpha1	43.28	0.78
Coix seed	MOL001494	Mandenol	42.00	0.19
Coix seed	MOL002372	(6Z,10E,14E,18E)-2,6,10,15,19,23-hexamethyltetracosa-2,6,10,14,18,22-hexaene	33.55	0.42
Coix seed	MOL002882	[(2R)-2,3-dihydroxypropyl] (Z)-octadec-9-enoate	34.13	0.30
Coix seed	MOL008118	Coixenolide	32.40	0.43
Coix seed	MOL008121	2-Monoolein	34.23	0.29
Morinda officinalis	MOL000358	beta-sitosterol	36.91	0.75
Morinda officinalis	MOL000359	sitosterol	36.91	0.75
Morinda officinalis	MOL001506	Supraene	33.55	0.42
Morinda officinalis	MOL002879	Diop	43.59	0.39
Morinda officinalis	MOL002883	Ethyl oleate (NF)	32.40	0.19
Morinda officinalis	MOL006147	Alizarin-2-methylether	32.81	0.21
Morinda officinalis	MOL009495	2-hydroxy-1,5-dimethoxy-6-(methoxymethyl)-9,10-anthraquinone	95.85	0.37
Morinda officinalis	MOL009496	1,5,7-trihydroxy-6-methoxy-2-methoxymethylanthracenequinone	80.42	0.38
Morinda officinalis	MOL009500	1,6-dihydroxy-5-methoxy-2-(methoxymethyl)-9,10-anthraquinone	104.54	0.34
Morinda officinalis	MOL009503	1-hydroxy-3-methoxy-9,10-anthraquinone	104.33	0.21

Morinda officinalis	MOL009504	1-hydroxy-6-hydroxymethylanthracenequinone	81.77	0.21
Morinda officinalis	MOL009513	2-hydroxy-1,8-dimethoxy-7-methoxymethylanthracenequinone	112.30	0.37
Morinda officinalis	MOL009519	(2R,3S)-(+)-3',5-Dihydroxy-4 ,7-dimethoxydihydroflavonol	77.24	0.33
Morinda officinalis	MOL009524	3beta,20(R),5-alkenyl-stigmastol	36.91	0.75
Morinda officinalis	MOL009525	3beta-24S(R)-butyl-5-alkenyl-cholestol	35.35	0.82
Morinda officinalis	MOL009537	americanin A	46.71	0.35
Morinda officinalis	MOL009541	Asperuloside tetraacetate	45.47	0.82
Morinda officinalis	MOL009551	isoprincepin	49.12	0.77
Morinda officinalis	MOL009558	2-hydroxyethyl 5-hydroxy-2-(2-hydroxybenzoyl)-4-(hydroxymethyl)benzoate	62.32	0.26
Morinda officinalis	MOL009562	Ohioensin-A	38.13	0.76
Epimedium	MOL000006	luteolin	36.16	0.25
Epimedium	MOL000098	quercetin	46.43	0.28
Epimedium	MOL000359	sitosterol	36.91	0.75
Epimedium	MOL000422	kaempferol	41.88	0.24
Epimedium	MOL000622	Magnograndiolide	63.71	0.19
Epimedium	MOL001510	24-epicampesterol	37.58	0.71
Epimedium	MOL001645	Linoleyl acetate	42.10	0.20
Epimedium	MOL001771	poriferast-5-en-3beta-ol	36.91	0.75
Epimedium	MOL001792	DFV	32.76	0.18
Epimedium	MOL003044	Chryseriol	35.85	0.27
Epimedium	MOL003542	8-Isopentenyl-kaempferol	38.04	0.39
Epimedium	MOL004367	olivil	62.23	0.41
Epimedium	MOL004373	Anhydroicaritin	45.41	0.44
Epimedium	MOL004380	C-Homoerythrinan, 1,6-didehydro-3,15,16-trimethoxy-, (3.beta.)-	39.14	0.49
Epimedium	MOL004382	Epimedium A	56.96	0.77
Epimedium	MOL004384	Epimedium C	45.67	0.50
Epimedium	MOL004386	Epimedium E	51.63	0.55
Epimedium	MOL004388	6-hydroxy-11,12-dimethoxy-2,2-dimethyl-1,8-dioxo-2,3,4,8-tetrahydro-1H-isochromeno[3,4-h]isoquinolin-2-ium	60.64	0.66
Epimedium	MOL004391	8-(3-methylbut-2-enyl)-2-phenyl-chromone	48.54	0.25
Epimedium	MOL004394	Anhydroicaritin-3-O-alpha-L-rhamnoside	41.58	0.61
Epimedium	MOL004396	1,2-bis(4-hydroxy-3-methoxyphenyl)propan-1,3-diol	52.31	0.22
Epimedium	MOL004425	Icariin	41.58	0.61
Epimedium	MOL004427	Icariside A7	31.91	0.86
Rhizoma Dioscoreae	MOL000310	Denudatin B	61.47	0.38
Rhizoma Dioscoreae	MOL000322	Kadsurenone	54.72	0.38
Rhizoma Dioscoreae	MOL000449	Stigmasterol	43.83	0.76
Rhizoma Dioscoreae	MOL000546	diosgenin	80.88	0.81
Rhizoma Dioscoreae	MOL000953	CLR	37.87	0.68
Rhizoma Dioscoreae	MOL001559	piperlonguminine	30.71	0.18
Rhizoma Dioscoreae	MOL001736	(-)-taxifolin	60.51	0.27
Rhizoma Dioscoreae	MOL005429	hancinol	64.01	0.37

Rhizoma Dioscoreae	MOL005430	hancinone C	59.05	0.39
Rhizoma Dioscoreae	MOL005435	24-Methylcholest-5-enyl-3belta-O-glucopyranoside_qt	37.58	0.72
Rhizoma Dioscoreae	MOL005438	campesterol	37.58	0.71
Rhizoma Dioscoreae	MOL005440	Isofucosterol	43.78	0.76
Rhizoma Dioscoreae	MOL005458	Dioscoreside C_qt	36.38	0.87
Rhizoma Dioscoreae	MOL005461	Doradexanthin	38.16	0.54
Rhizoma Dioscoreae	MOL005463	Methylcimicifugoside_qt	31.69	0.24
Rhizoma Dioscoreae	MOL005465	AIDS180907	45.33	0.77
Astragalus membranaceus	MOL000033	(3S,8S,9S,10R,13R,14S,17R)-10,13-dimethyl-17-[(2R,5S)-5-propan-2-yloctan-2-yl]-2,3,4,7,8,9,11,12,14,15,16,17-dodecahydro-1H-cyclopenta[a]phenanthren-3-ol	36.23	0.78
Astragalus membranaceus	MOL000098	quercetin	46.43	0.28
Astragalus membranaceus	MOL000211	Mairin	55.38	0.78
Astragalus membranaceus	MOL000239	Jaranol	50.83	0.29
Astragalus membranaceus	MOL000296	hederagenin	36.91	0.75
Astragalus membranaceus	MOL000354	isorhamnetin	49.60	0.31
Astragalus membranaceus	MOL000371	3,9-di-O-methylnissolin	53.74	0.48
Astragalus membranaceus	MOL000374	5'-hydroxyiso-muronulatol-2',5'-di-O-glucoside	41.72	0.69
Astragalus membranaceus	MOL000378	7-O-methylisomucronulatol	74.69	0.30
Astragalus membranaceus	MOL000379	9,10-dimethoxypterocarpan-3-O-β-D-glucoside	36.74	0.92
Astragalus membranaceus	MOL000380	(6aR,11aR)-9,10-dimethoxy-6a,11a-dihydro-6H-benzofurano[3,2-c]chromen-3-ol	64.26	0.42
Astragalus membranaceus	MOL000387	Bifendate	31.10	0.67
Astragalus membranaceus	MOL000392	formononetin	69.67	0.21
Astragalus membranaceus	MOL000398	isoflavanone	109.99	0.30
Astragalus membranaceus	MOL000417	Calycosin	47.75	0.24
Astragalus membranaceus	MOL000422	kaempferol	41.88	0.24
Astragalus membranaceus	MOL000433	FA	68.96	0.71
Astragalus membranaceus	MOL000438	(3R)-3-(2-hydroxy-3,4-dimethoxyphenyl)chroman-7-ol	67.67	0.26
Astragalus membranaceus	MOL000439	isomucronulatol-7,2'-di-O-glucosiole	49.28	0.62
Astragalus membranaceus	MOL000442	1,7-Dihydroxy-3,9-dimethoxy pterocarpene	39.05	0.48
Cassia twig	MOL001736	(-)-taxifolin	60.51	0.27
Cassia twig	MOL000358	beta-sitosterol	36.91	0.75
Cassia twig	MOL000359	sitosterol	36.91	0.75
Cassia twig	MOL000492	(+)-catechin	54.83	0.24
Cassia twig	MOL000073	ent-Epicatechin	48.96	0.24
Cassia twig	MOL004576	taxifolin	57.84	0.27
Cassia twig	MOL011169	Peroxyergosterol	44.39	0.82

Poria cocos	MOL000273	(2R)-2-[(3S,5R,10S,13R,14R,16R,17R)-3,16-dihydroxy-4,4,10,13,14-pentamethyl-2,3,5,6,12,15,16,17-octahydro-1H-cyclopenta[a]phenanthren-17-yl]-6-methylhept-5-enoic acid	30.93	0.81
Poria cocos	MOL000275	trametenolic acid	38.71	0.80
Poria cocos	MOL000276	7,9(11)-dehydropachymic acid	35.11	0.81
Poria cocos	MOL000279	Cerevisterol	37.96	0.77
Poria cocos	MOL000280	(2R)-2-[(3S,5R,10S,13R,14R,16R,17R)-3,16-dihydroxy-4,4,10,13,14-pentamethyl-2,3,5,6,12,15,16,17-octahydro-1H-cyclopenta[a]phenanthren-17-yl]-5-isopropyl-hex-5-enoic acid	31.07	0.82
Poria cocos	MOL000282	ergosta-7,22E-dien-3beta-ol	43.51	0.72
Poria cocos	MOL000283	Ergosterol peroxide	40.36	0.81
Poria cocos	MOL000285	(2R)-2-[(5R,10S,13R,14R,16R,17R)-16-hydroxy-3-keto-4,4,10,13,14-pentamethyl-1,2,5,6,12,15,16,17-octahydrocyclopenta[a]phenanthren-17-yl]-5-isopropyl-hex-5-enoic acid	38.26	0.82
Poria cocos	MOL000287	3beta-Hydroxy-24-methylene-8-lanostene-21-oic acid	38.70	0.81
Poria cocos	MOL000289	pachymic acid	33.63	0.81
Poria cocos	MOL000290	Poricoic acid A	30.61	0.76
Poria cocos	MOL000291	Poricoic acid B	30.52	0.75
Poria cocos	MOL000292	poricoic acid C	38.15	0.75
Poria cocos	MOL000296	hederagenin	36.91	0.75
Poria cocos	MOL000300	dehydroeburicoic acid	44.17	0.83
Codonopsis pilosula	MOL000006	luteolin	36.16	0.25
Codonopsis pilosula	MOL000449	Stigmasterol	43.83	0.76
Codonopsis pilosula	MOL001006	poriferasta-7,22E-dien-3beta-ol	42.98	0.76
Codonopsis pilosula	MOL002140	Perlolyrine	65.95	0.27
Codonopsis pilosula	MOL002879	Diop	43.59	0.39
Codonopsis pilosula	MOL003036	ZINC03978781	43.83	0.76
Codonopsis pilosula	MOL003896	7-Methoxy-2-methyl isoflavone	42.56	0.20
Codonopsis pilosula	MOL004355	Spinasterol	42.98	0.76
Codonopsis pilosula	MOL004492	Chrysanthemaxanthin	38.72	0.58
Codonopsis pilosula	MOL005321	Frutinone A	65.90	0.34
Codonopsis pilosula	MOL006554	Taraxerol	38.40	0.77
Codonopsis pilosula	MOL006774	stigmast-7-enol	37.42	0.75
Codonopsis pilosula	MOL007059	3-beta-Hydroxymethyllenetanshiquinone	32.16	0.41
Codonopsis pilosula	MOL007514	methyl icosa-11,14-dienoate	39.67	0.23
Codonopsis pilosula	MOL008391	5alpha-Stigmastan-3,6-dione	33.12	0.79
Codonopsis pilosula	MOL008393	7-(beta-Xylosyl)cephalomannine_qt	38.33	0.29
Codonopsis pilosula	MOL008397	Daturilin	50.37	0.77
Codonopsis pilosula	MOL008400	glycitein	50.48	0.24
Codonopsis pilosula	MOL008406	Spinoside A	39.97	0.40
Codonopsis pilosula	MOL008407	(8S,9S,10R,13R,14S,17R)-17-[(E,2R,5S)-5-ethyl-6-methylhept-3-en-2-yl]-10,13-dimethyl-1,2,4,7,8,9,11,12,14,15,16,17-dodecahydrocyclopenta[a]phenanthren-3-one	45.40	0.76

Codonopsis pilosula	MOL008411	11-Hydroxyrankinidine	40.00	0.66
Pinellia ternata	MOL000358	beta-sitosterol	36.91	0.75
Pinellia ternata	MOL000449	Stigmasterol	43.83	0.76
Pinellia ternata	MOL000519	coniferin	31.11	0.32
Pinellia ternata	MOL001755	24-Ethylcholest-4-en-3-one	36.08	0.76
Pinellia ternata	MOL002670	Cavidine	35.64	0.81
Pinellia ternata	MOL002714	baicalein	33.52	0.21
Pinellia ternata	MOL002776	Baicalin	40.12	0.75
Pinellia ternata	MOL003578	Cycloartenol	38.69	0.78
Pinellia ternata	MOL005030	gondoic acid	30.70	0.20
Pinellia ternata	MOL006936	10,13-eicosadienoic	39.99	0.20
Pinellia ternata	MOL006937	12,13-epoxy-9-hydroxynonadeca-7,10-dienoic acid	42.15	0.24
Pinellia ternata	MOL006957	(3S,6S)-3-(benzyl)-6-(4-hydroxybenzyl)piperazine-2,5-quinone	46.89	0.27
Pinellia ternata	MOL006967	beta-D-Ribofuranoside, xanthine-9	44.72	0.21
Licorice	MOL001484	Inermine	75.18	0.54
Licorice	MOL001792	DFV	32.76	0.18
Licorice	MOL000211	Mairin	55.38	0.78
Licorice	MOL002311	Glycyrol	90.78	0.67
Licorice	MOL000239	Jaranol	50.83	0.29
Licorice	MOL002565	Medicarpin	49.22	0.34
Licorice	MOL000354	isorhamnetin	49.60	0.31
Licorice	MOL000359	sitosterol	36.91	0.75
Licorice	MOL003656	Lupiwighteone	51.64	0.37
Licorice	MOL003896	7-Methoxy-2-methyl isoflavone	42.56	0.20
Licorice	MOL000392	formononetin	69.67	0.21
Licorice	MOL000417	Calycosin	47.75	0.24
Licorice	MOL000422	kaempferol	41.88	0.24
Licorice	MOL004328	naringenin	59.29	0.21
Licorice	MOL004805	(2S)-2-[4-hydroxy-3-(3-methylbut-2-enyl)phenyl]-8,8-dimethyl-2,3-dihydropyrano[2,3-f]chromen-4-one	31.79	0.72
Licorice	MOL004806	euchrenone	30.29	0.57
Licorice	MOL004808	glyasperin B	65.22	0.44
Licorice	MOL004810	glyasperin F	75.84	0.54
Licorice	MOL004811	Glyasperin C	45.56	0.40
Licorice	MOL004814	Isotrifoliol	31.94	0.42
Licorice	MOL004815	(E)-1-(2,4-dihydroxyphenyl)-3-(2,2-dimethylchromen-6-yl)prop-2-en-1-one	39.62	0.35
Licorice	MOL004820	kanzonols W	50.48	0.52
Licorice	MOL004824	(2S)-6-(2,4-dihydroxyphenyl)-2-(2-hydroxypropan-2-yl)-4-methoxy-2,3-dihydrofuro[3,2-g]chromen-7-one	60.25	0.63
Licorice	MOL004827	Semilicoisoflavone B	48.78	0.55
Licorice	MOL004828	Glepidotin A	44.72	0.35
Licorice	MOL004829	Glepidotin B	64.46	0.34
Licorice	MOL004833	Phaseolinisoflavan	32.01	0.45
Licorice	MOL004835	Glypallichalcone	61.60	0.19

Licorice	MOL004838	8-(6-hydroxy-2-benzofuranyl)-2,2-dimethyl-5-chromenol	58.44	0.38
Licorice	MOL004841	Licochalcone B	76.76	0.19
Licorice	MOL004848	licochalcone G	49.25	0.32
Licorice	MOL004849	3-(2,4-dihydroxyphenyl)-8-(1,1-dimethylprop-2-enyl)-7-hydroxy-5-methoxy-coumarin	59.62	0.43
Licorice	MOL004855	Licoricone	63.58	0.47
Licorice	MOL004856	Gancaonin A	51.08	0.40
Licorice	MOL004857	Gancaonin B	48.79	0.45
Licorice	MOL004860	licorice glycoside E	32.89	0.27
Licorice	MOL004863	3-(3,4-dihydroxyphenyl)-5,7-dihydroxy-8-(3-methylbut-2-enyl)chromone	66.37	0.41
Licorice	MOL004864	5,7-dihydroxy-3-(4-methoxyphenyl)-8-(3-methylbut-2-enyl)chromone	30.49	0.41
Licorice	MOL004866	2-(3,4-dihydroxyphenyl)-5,7-dihydroxy-6-(3-methylbut-2-enyl)chromone	44.15	0.41
Licorice	MOL004879	Glycyrin	52.61	0.47
Licorice	MOL004882	Licocoumarone	33.21	0.36
Licorice	MOL004883	Licoisoflavone	41.61	0.42
Licorice	MOL004884	Licoisoflavone B	38.93	0.55
Licorice	MOL004885	licoisoflavanone	52.47	0.54
Licorice	MOL004891	shinpterocarpin	80.30	0.73
Licorice	MOL004898	(E)-3-[3,4-dihydroxy-5-(3-methylbut-2-enyl)phenyl]-1-(2,4-dihydroxyphenyl)prop-2-en-1-one	46.27	0.31
Licorice	MOL004903	liquiritin	65.69	0.74
Licorice	MOL004904	licopyranocoumarin	80.36	0.65
Licorice	MOL004905	3,22-Dihydroxy-11-oxo-delta(12)-oleanene-27-alpha-methoxycarbonyl-29-oic acid	34.32	0.55
Licorice	MOL004907	Glyzaglabrin	61.07	0.35
Licorice	MOL004908	Glabridin	53.25	0.47
Licorice	MOL004910	Glabranin	52.90	0.31
Licorice	MOL004911	Glabrene	46.27	0.44
Licorice	MOL004912	Glabrone	52.51	0.50
Licorice	MOL004913	1,3-dihydroxy-9-methoxy-6-benzofurano[3,2-c]chromenone	48.14	0.43
Licorice	MOL004914	1,3-dihydroxy-8,9-dimethoxy-6-benzofurano[3,2-c]chromenone	62.90	0.53
Licorice	MOL004915	Eurycarpin A	43.28	0.37
Licorice	MOL004917	glycyroside	37.25	0.79
Licorice	MOL004924	(-)-Medicocarpin	40.99	0.95
Licorice	MOL004935	Sigmoidin-B	34.88	0.41
Licorice	MOL004941	(2R)-7-hydroxy-2-(4-hydroxyphenyl)chroman-4-one	71.12	0.18
Licorice	MOL004945	(2S)-7-hydroxy-2-(4-hydroxyphenyl)-8-(3-methylbut-2-enyl)chroman-4-one	36.57	0.32
Licorice	MOL004948	Isoglycyrol	44.70	0.84
Licorice	MOL004949	Isolicoflavonol	45.17	0.42
Licorice	MOL004957	HMO	38.37	0.21
Licorice	MOL004959	1-Methoxyphaseollidin	69.98	0.64
Licorice	MOL004961	Quercetin der.	46.45	0.33
Licorice	MOL004966	3'-Hydroxy-4'-O-Methylglabridin	43.71	0.57
Licorice	MOL000497	licochalcone a	40.79	0.29
Licorice	MOL004974	3'-Methoxyglabridin	46.16	0.57
Licorice	MOL004978	2-[(3R)-8,8-dimethyl-3,4-dihydro-2H-pyrano[6,5-f]chromen-3-yl]-5-methoxyphenol	36.21	0.52
Licorice	MOL004980	Inflacoumarin A	39.71	0.33
Licorice	MOL004985	icos-5-enoic acid	30.70	0.20
Licorice	MOL004988	Kanzonol F	32.47	0.89
Licorice	MOL004989	6-prenylated eriodictyol	39.22	0.41

Licorice	MOL004990	7,2',4'-trihydroxy□5-methoxy-3□arylcoumarin	83.71	0.27
Licorice	MOL004991	7-Acetoxy-2-methylisoflavone	38.92	0.26
Licorice	MOL004993	8-prenylated eriodictyol	53.79	0.40
Licorice	MOL004996	gadelaidic acid	30.70	0.20
Licorice	MOL000500	Vestitol	74.66	0.21
Licorice	MOL005000	Gancaonin G	60.44	0.39
Licorice	MOL005001	Gancaonin H	50.10	0.78
Licorice	MOL005003	Licoagrocarpin	58.81	0.58
Licorice	MOL005007	Glyasperins M	72.67	0.59
Licorice	MOL005008	Glycyrrhiza flavonol A	41.28	0.60
Licorice	MOL005012	Licoagroisoflavone	57.28	0.49
Licorice	MOL005013	18α-hydroxyglycyrrhetic acid	41.16	0.71
Licorice	MOL005016	Odoratin	49.95	0.30
Licorice	MOL005017	Phaseol	78.77	0.58
Licorice	MOL005018	Xambioona	54.85	0.87
Licorice	MOL005020	dehydroglyasperins C	53.82	0.37
Licorice	MOL000098	quercetin	46.43	0.28

Table 2. The first 20 genes that are upregulated and downregulated.

Gene names	logFC	P.Value	Regulation direction
PPP1R14A	1.962420783	8.76E-06	Up
GATA3	1.092763592	0.000113749	Up
OOSP2	0.920223801	0.00016017	Up
CCDC3	1.974333764	0.000196378	Up
NANOS1	1.103302823	0.000232374	Up
LOC100653086	2.66416782	0.000436055	Up
RBM46	0.63266134	0.000446411	Up
CD151	0.842862532	0.000473413	Up
FOXE1	0.726611457	0.000508009	Up
TAAR8	0.683366979	0.00051555	Up
RP11-426C22.5	0.953960371	0.000565624	Up
TTC16	1.416136477	0.000577946	Up
INVS	0.524518869	0.000619569	Up
LOC285819	1.2797932	0.000628609	Up
LNX2	0.913871461	0.000639599	Up
GZMH	1.053802376	0.000765797	Up
APOL3	0.64050562	0.000842817	Up
CBFA2T3	0.666327167	0.000850395	Up
KB-1410C5.2	0.926477738	0.000923285	Up
COX7A1	1.286833415	0.000981155	Up
CD19	-1.20795632	3.35E-05	Down
DSEL	-0.96197409	8.39E-05	Down
PSD4	-0.88241727	9.63E-05	Down
LOC101929118	-1.06251656	0.000193503	Down
TDRG1	-0.69988508	0.000218897	Down
CELF2-AS1	-0.92543113	0.00031045	Down
DNAJC5G	-1.07240457	0.000510068	Down
LOC100505727	-0.92204444	0.000661223	Down
3-Sep	-1.50595321	0.000699132	Down
RP11-214N1.1	-0.60951434	0.000908948	Down
NEURL2	-1.01281867	0.000999084	Down
SMTN	-0.50887956	0.001135325	Down
SLIT2-IT1	-0.97264748	0.001159109	Down
LOC101927798	-0.91607571	0.001167393	Down
EPHB3	-1.00615294	0.001196516	Down
LYVE1	-1.08553386	0.001268906	Down
SERPINE2	-0.94688536	0.001282605	Down
LINC00282	-1.14851345	0.001291206	Down
GPC4	-0.70092615	0.001375031	Down
PFKFB2	-0.75911483	0.001546603	Down

Table 3. The 13 intersection genes sorted by logFC

Intersection gene	logFC	P.Value
NQO1	1.820074114	0.001932798
ADRB2	0.86137564	0.004854359
ADRA2A	0.810192522	0.038152075
AKR1C1	0.799433273	0.002184945
ADRA2C	0.746382332	0.003191618
IRF1	0.561582599	0.029696511
CHEK1	-0.606745591	0.013406924
TIMP1	-0.615485931	0.029365414
PCOLCE	-0.715802695	0.048929664
PLAU	-0.766865977	0.026001005
CHEK2	-0.806131966	0.003795712
DGAT2	-1.146794214	0.01797957
PLAT	-1.472074459	0.021764444

Table 4. Topological analysis results by degree—the first 30 proteins

Genename	Annotation	Degree	Betweenness
ADRB2	adrenoceptor beta 2	258	3.963547237
TP53	tumor protein p53	147	52.86383645
FN1	fibronectin 1	126	24.06731908
UBC	ubiquitin C	118	31.70379518
YWHAZ	tyrosine 3-monooxygenase/tryptophan 5-monooxygenase activation protein zeta	104	33.58273977
FBXO6	F-box protein 6	103	4.556352591
COPS5	COP9 signalosome subunit 5	103	16.45314159
CHEK2	checkpoint kinase 2	100	2.579215229
HSP90AA1	heat shock protein 90 alpha family class A member 1	100	29.86419496
ITGA4	integrin subunit alpha 4	100	6.993295387
MYC	v-myc avian myelocytomatosis viral oncogene homolog	98	13.680114
APP	amyloid beta precursor protein	97	19.88249806
NPM1	nucleophosmin	94	34.43407312
CHEK1	checkpoint kinase 1	93	14.23246476
VCP	valosin containing protein	91	44.94481576
HSPA5	heat shock protein family A (Hsp70) member 5	90	27.04402901
EP300	E1A binding protein p300	88	18.09652374
BRCA1	BRCA1, DNA repair associated	85	14.46620487
GRB2	growth factor receptor bound protein 2	85	12.69787382
CUL1	cullin 1	85	28.06120574
HSP90AB1	heat shock protein 90 alpha family class B member 1	84	17.79113076
MDM2	MDM2 proto-oncogene	84	37.37250751
EEF1A1	eukaryotic translation elongation factor 1 alpha 1	74	22.86009248
CUL2	cullin 2	73	9.883269792
FUS	FUS RNA binding protein	70	13.36597597
PCNA	proliferating cell nuclear antigen	69	18.81042846
RPA2	replication protein A2	68	10.70812663
AKT1	AKT serine/threonine kinase 1	67	17.61139498

Table 5. The enrichment pathways corresponding to intersection genes

Term	Description	Count	GeneID	BgRatio
hsa04022	cGMP-PKG signaling pathway	3	ADRB2/ADRA2C/ADRA2A	167/8108
hsa04115	p53 signaling pathway	2	CHEK1/CHEK2	73/8108
hsa04610	Complement and coagulation cascades	2	PLAU/PLAT	85/8108
hsa05215	Prostate cancer	2	PLAU/PLAT	97/8108
hsa04080	Neuroactive ligand-receptor interaction	3	ADRB2/ADRA2C/ADRA2A	341/8108
hsa04110	Cell cycle	2	CHEK1/CHEK2	124/8108
hsa00130	Ubiquinone and other terpenoid-quinone biosynthesis	1	NQO1	11/8108
hsa05418	Fluid shear stress and atherosclerosis	2	PLAT/NQO1	139/8108
hsa04218	Cellular senescence	2	CHEK1/CHEK2	156/8108

Table 6. Binding energies of MLGZG's key components to the target gene molecules

mponents	Binding energies (kcal/mol)								
	ADRB2	DGAT2	ADRA2A	ADRA2C	CHEK2	NQO1	CHEK1	PLAU	PLAT
nisoflavan	-10.3	-10.1	-9.5	-9.3	-9.3	-9	-8.8	-7.8	-7.7
roicaritin	-9.9	-9.5	-9.1	-9.6	-10.1	-8.6	-8.2	-6.9	-7.6
rcetin	-9.2	-7.5	-8.9	-9.3	-9.2	-8.1	-8	-7.5	-8.1
asterol	-8.6	-8.4	-8.4	-9.5	-7.7	-10.2	-6.4	-7.2	-7.1
nonetin	-7.8	-7.5	-8.9	-8.8	-9	-7.9	-7.3	-6.5	-6.8
ycosin	-7.8	-7	-7.3	-8.5	-9.1	-8.3	-7.6	-6.8	-7.4
iletin	-7.1	-6.6	-7.6	-8.1	-7.9	-8.1	-7.1	-6.1	-6
thrinan, 1,6- o-3,15,16- y-, (3.beta.)-	-6.8	-6.7	-7.3	-7.5	-6	-7.8	-6.1	-6.7	-6.6
omucronulatol	-6.3	-8.8	-8.2	-8.7	-8.5	-7.7	-7.2	-6.6	-6.4
idine	-5.2	-8.4	-8.4	-9	-8.3	-9.2	-8.2	-7.2	-7.2

Figures

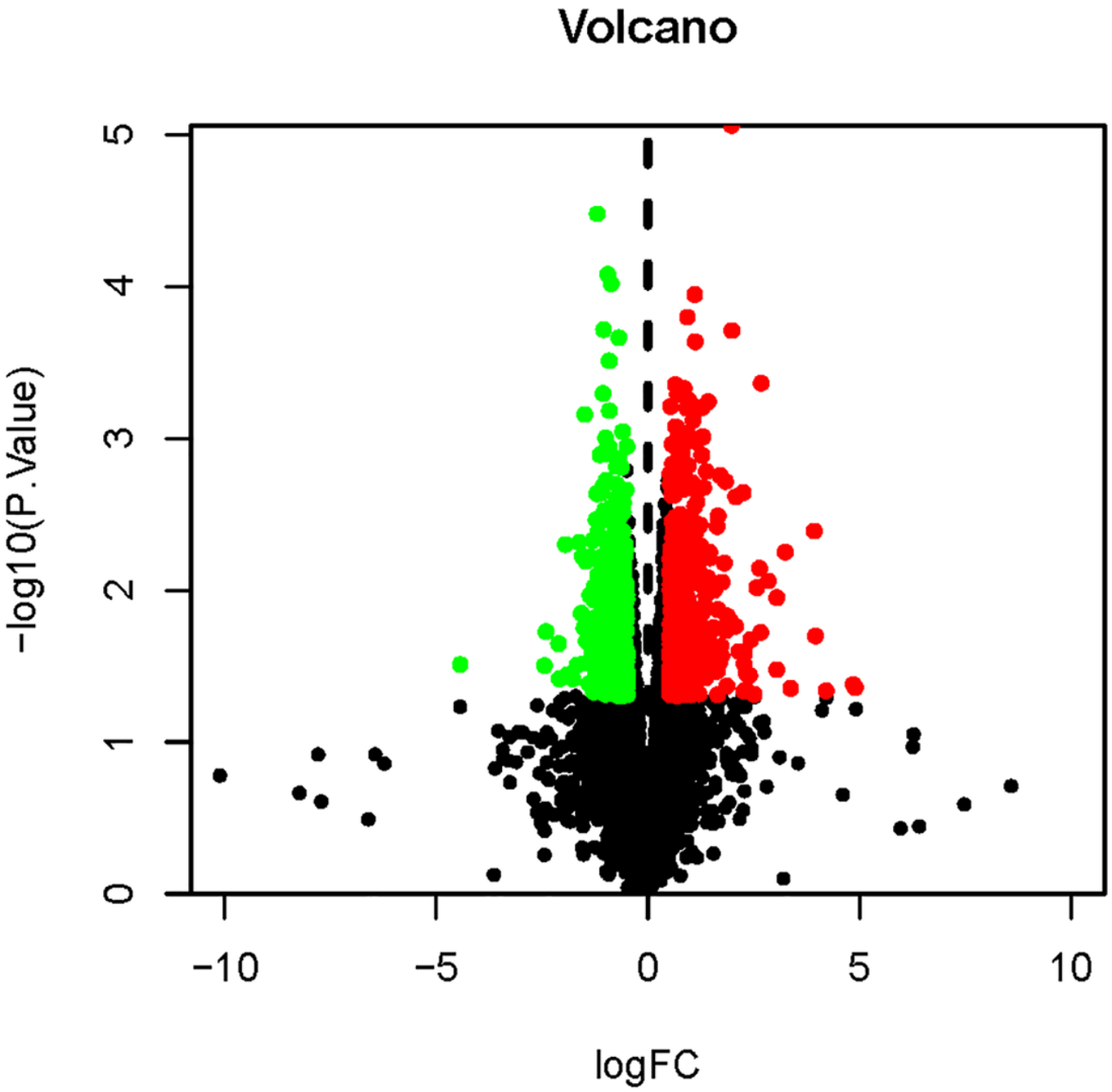

Figure 1

Gene volcano map shows the gene distribution in disease samples. Red and green represent upregulated genes (logFC > 0) and downregulated genes (logFC < 0), respectively, whereas black indicates no significant difference.

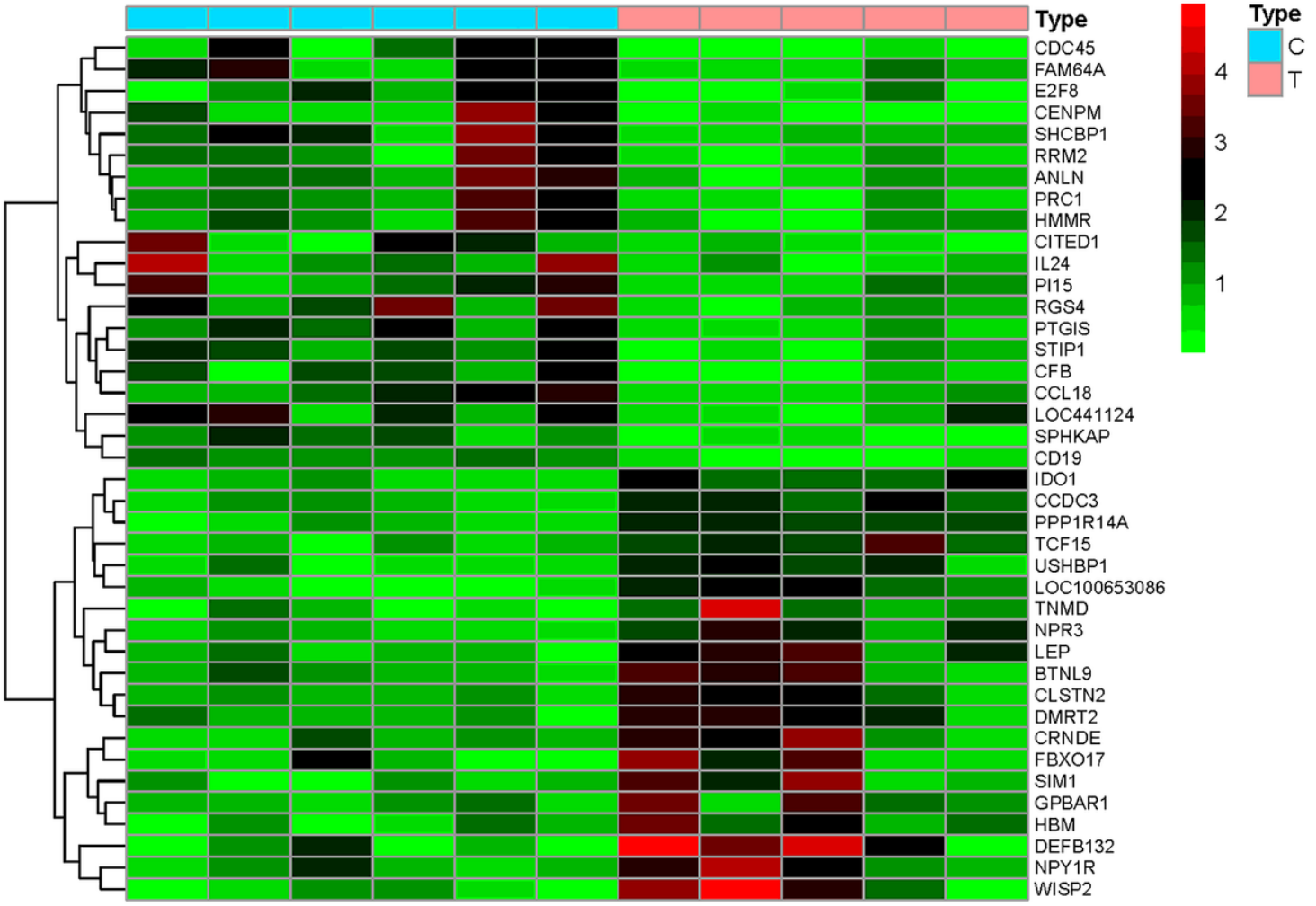

Figure 2

Gene heat map. In the gene heat map, red and green represent upregulated (logFC > 0) and downregulated (logFC < 0) genes in the sample, respectively, whereas black represents no significant difference. The first eight samples were from healthy people and the last seven samples were from obese patients.

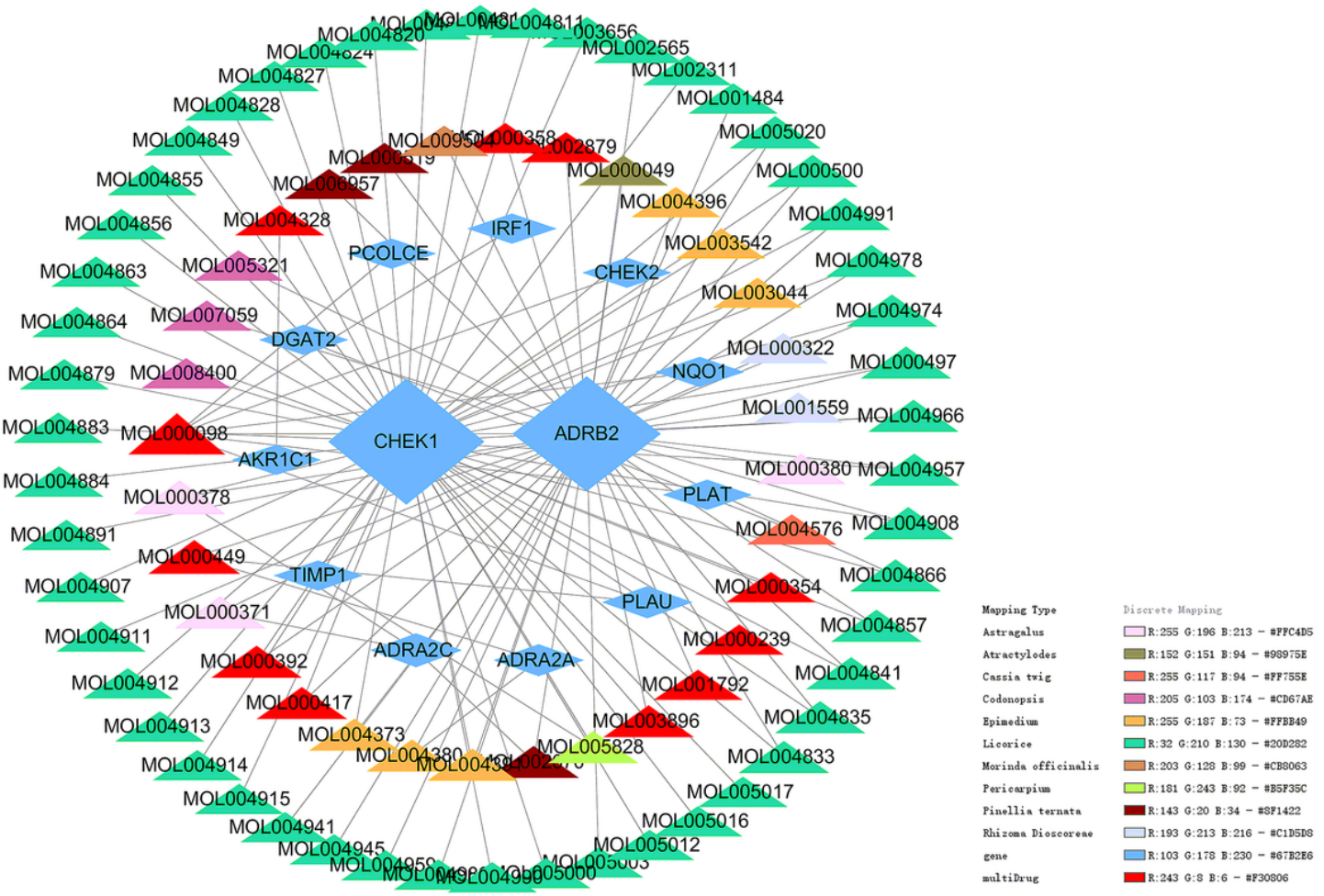

Figure 3

TCM compound-disease regulatory network. This network shows the targeted relationship between the active components of TCM and the intersection genes.

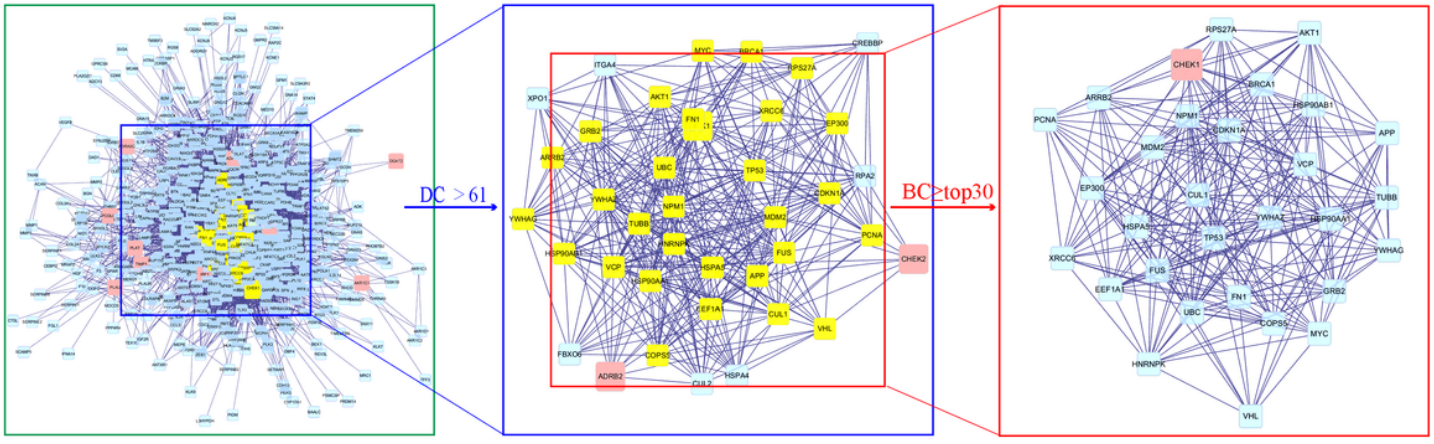

Figure 4

Topological analysis of the protein-protein interaction network. Herein, 580 protein nodes were obtained according to the intersection genes. After screening by DC > 61 for the first time, a total of 39 protein nodes were obtained, and the first 30 proteins were extracted according to BC for the second time.

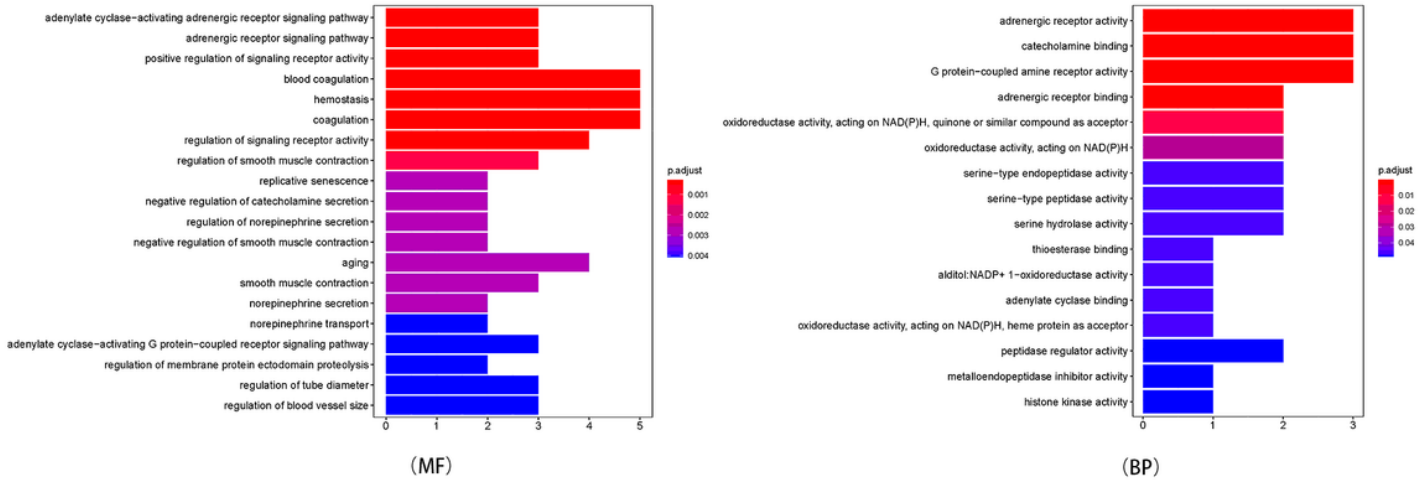

Figure 5

GO enrichment analysis of JW-LZD targets in treating obesity. The horizontal axis of the BP and MF column represents the number of genes enriched in each item, and the color represents the enrichment significance based on the corrected P value.

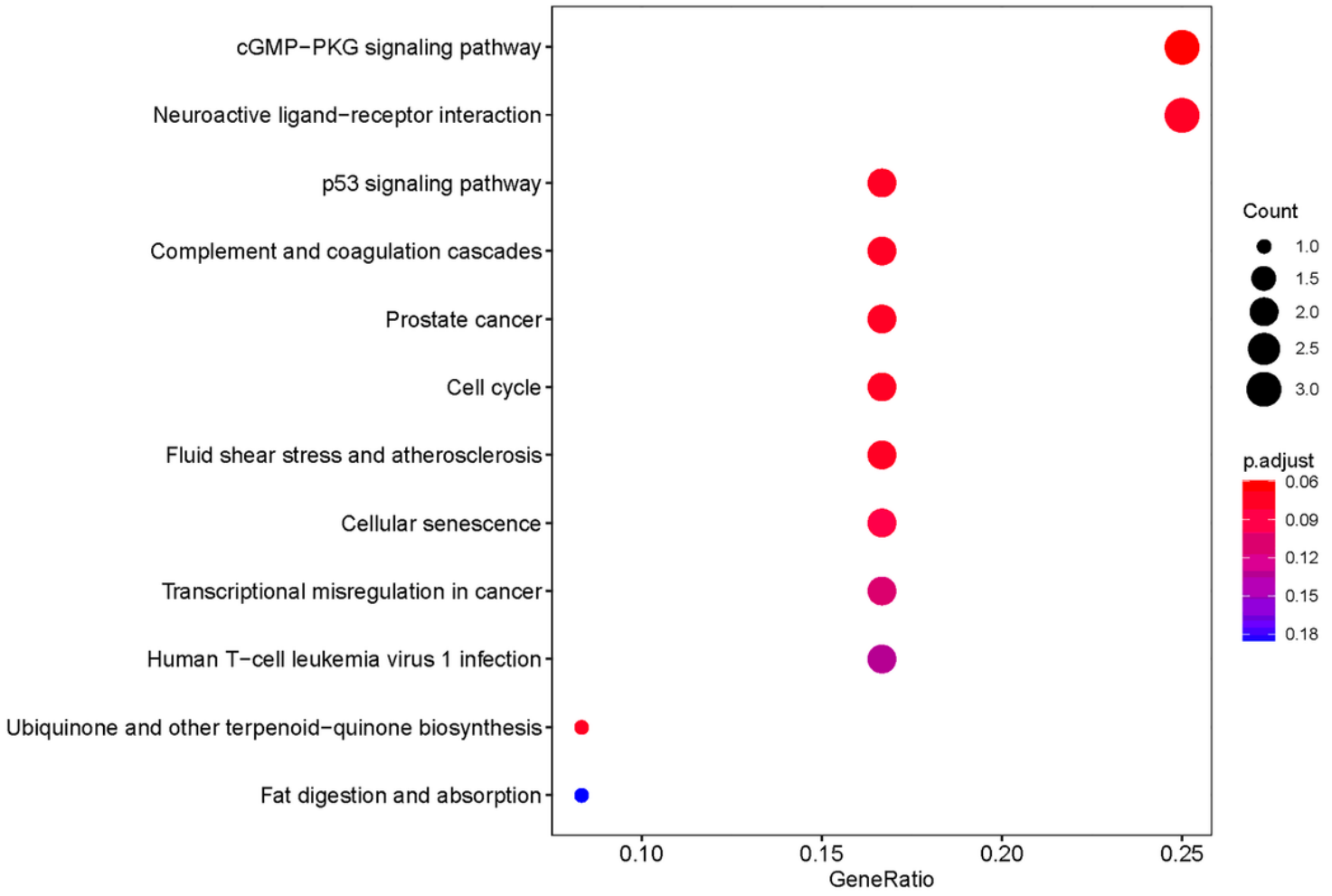

Figure 6

KEGG bubble. The horizontal axis of the KEGG bubble diagram represents the gene proportion enriched in each entry, and the vertical axis shows the enrichment degree according to the corrected P value.

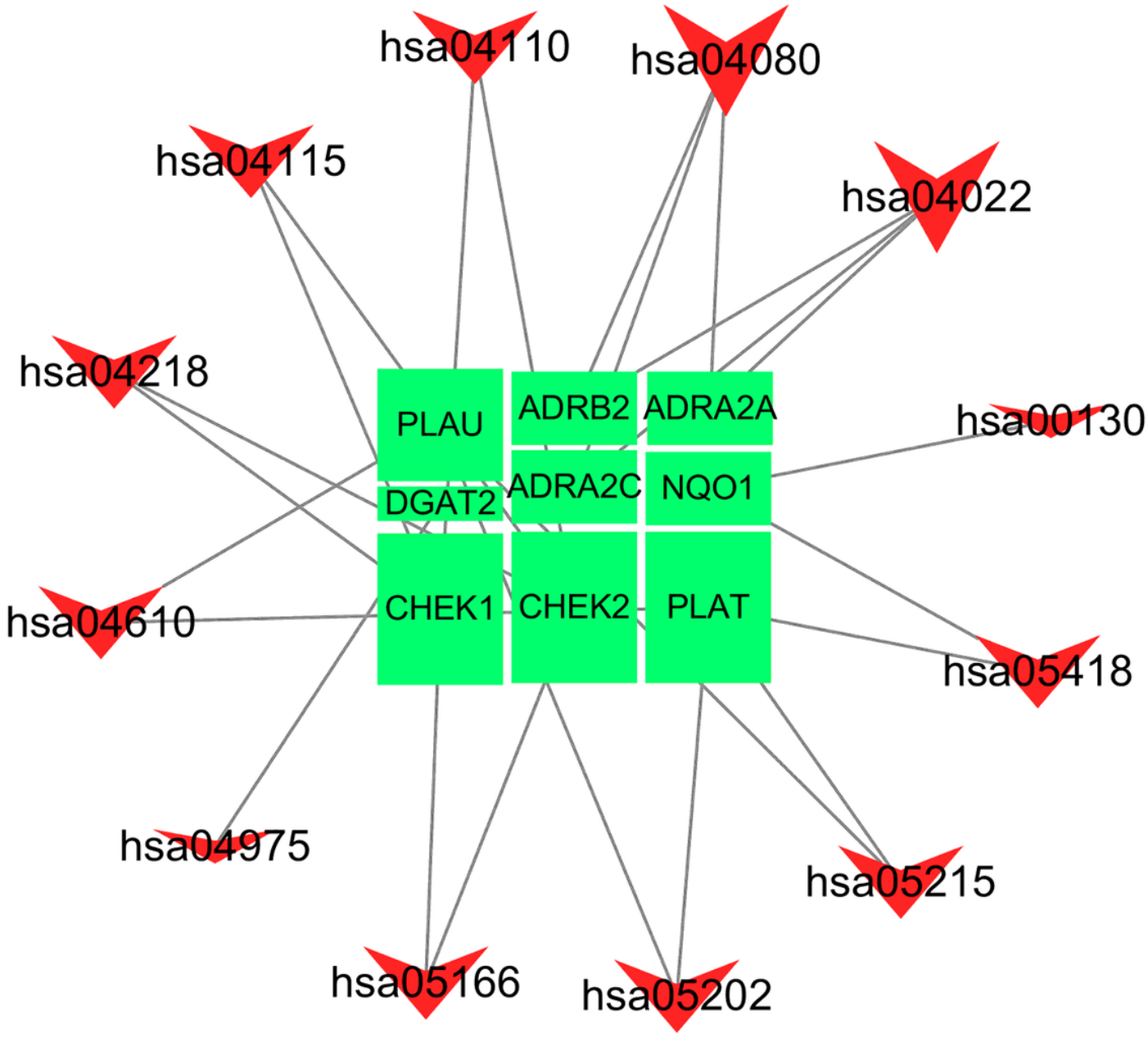

Figure 7

KEGG relational regulatory network. This network shows the relationship between the enriched 12 pathways and 9 genes, and the size of the graph shows the number of pathways or genes connected.

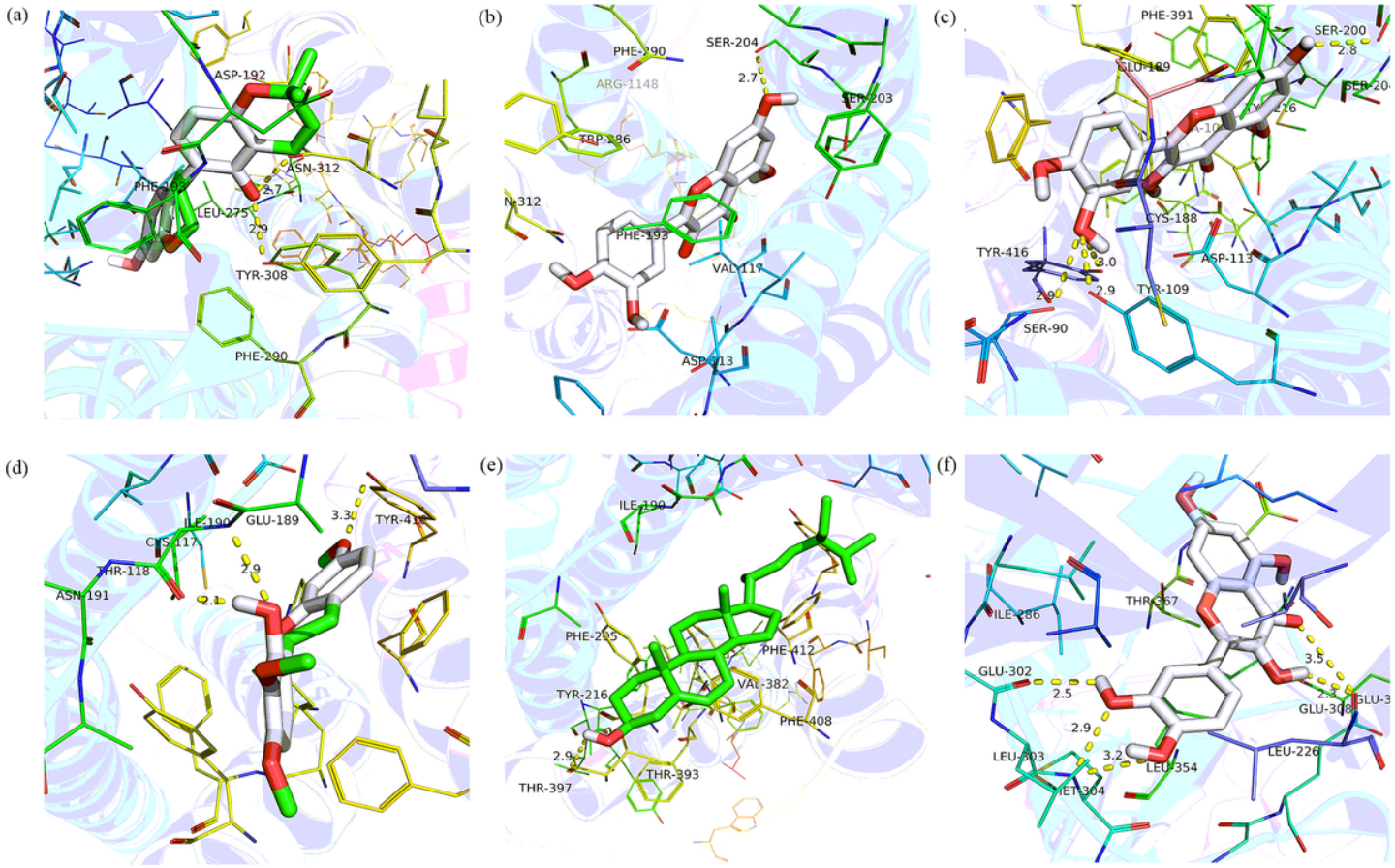

Figure 8

Partial diagram of molecular docking: (a) ADRB2-Phaseolinisoflavan; (b) ADRB2-quercetin; (c) ADRA2A-quercetin; (d) ADRA2A-7-O-methylisomucronulatol; (e) ADRA2A-Stigmasterol; (f) CHECK2-quercetin;